ACS Photonics

pubs.acs.org/journal/apchd5

Article

Photonic Topological Baths for Quantum Simulation

Abhi Saxena,* Yueyang Chen, Zhuoran Fang, and Arka Majumdar*

Cite This: https://doi.org/10.1021/acsphotonics.1c01751

Read Online

ACCESS | Metrics & More | Article Recommendations | Supporting Information

ABSTRACT: Quantum simulation involves engineering devices to implement different Hamiltonians and measuring their quantized spectra to study quantum many-body systems. Recent developments in topological photonics have shown the possibility of studying novel quantum phenomena by controlling the topological properties of such devices. Here, using coupled arrays of up to 16 high Q silicon nanocavities, we experimentally realize quantum photonic baths, which are analogs of the Su−Schrieffer−Heeger model. We investigate the effect of fabrication-induced disorder on these baths by probing individual supermodes. We further demonstrate the design mitigation steps required to overcome the disorder effects in photonic cavities to simulate quantum systems.

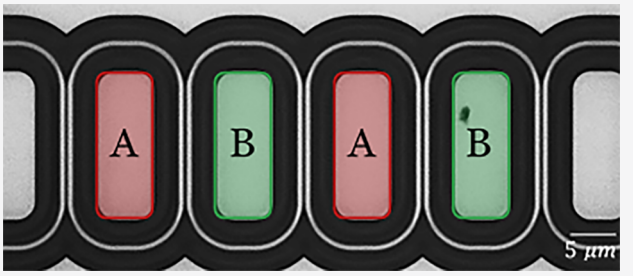

KEYWORDS: *quantum simulation, topological photonics, coupled cavity array*

Use of photons as particles in controlled quantum systems to study other complex nonequilibrium quantum phenomenon forms the basis of one of the most promising paradigms for quantum simulation.[1−5] This typically involves implementing Hamiltonians by engineering coupled photonic resonators to tailor photons energy momentum relationships.[6,7] Recent advances in controlling topological properties of photonic lattices have shown that novel forms of light−matter interaction can be realized in such systems owing to the topological protection of the resulting quantum many body states.[8−11] While the microwave photons in superconducting circuits have already been used to exhibit these unconventional quantum phenomena,[12] such a demonstration is missing in optical domain. Observing similar effects in optics will not only significantly simplify the experiments due to performability at much higher temperatures but will also allow measurements of multiparticle correlations due to the availability of single photon detectors. In fact, recent demonstrations of large-scale photonic quantum computers attest to such inherent scalability of photonics.[13,14] To reach this regime of interacting photons for quantum simulation in optical domain we need to implement the topological phases on photonic lattices made with high quality (Q) factor and low mode volume resonators with spectral accessibility to individual super modes.[15] However, due to unavoidable imperfections in nanofabrication, high Q optical resonator arrays are inherently prone to disorder in their resonant frequencies. Without undertaking suitable mitigating steps in design of these arrays, this uncontrolled disorder can be a serious impediment in constructing topological baths suitable for studying various quantum optical phenomena. Typical coupled cavity arrays used to demonstrate topological states in the optical domain[16−23] operate in a regime where fabrication induced disorder is comparable or greater than the relevant hopping rates between the cavities. While such a regime is sufficient for observing the topological modes, it is not suitable for estimating all the parameters of a Hamiltonian, as needed for quantum simulation. In this paper, by increasing the effective mode overlap between resonators sites we overcame the effects of the underlying disorder and experimentally realized topological quantum electrodynamic baths, which are photonic analogs of the Su−Schrieffer−Heeger (SSH) model.[24] We show that these coupled cavity array baths (with individual Q-factor exceeding 3.1×10^4) operate in a regime which is suitable for quantum simulation and can be used to impart special topological properties to interacting photons as discussed in depth by Bello et al.[8]

DESCRIPTION OF THE SSH PHOTONIC BATH

The SSH model describing the topological photonic bath is illustrated in Figure 1a. The photonic lattice consists of sublattices A and B of the array, respectively, made up of cavities with resonant frequency ω_0. The intracell hopping rate between the sites A and B of a unit cell is given by J_1 and the intercell hopping rate between the unit cells is denoted by J_2. The Hamiltonian of this bath can be written as ($\hbar = 1$)

$$\mathcal{H}_B = \sum_i \omega_0(a_i^\dagger a_i + b_i^\dagger b_i) + J_1(b_i^\dagger a_i + a_i^\dagger b_i) + J_2(b_i^\dagger a_{i+1} + a_{i+1}^\dagger b_i) \quad (1)$$

Received: November 15, 2021

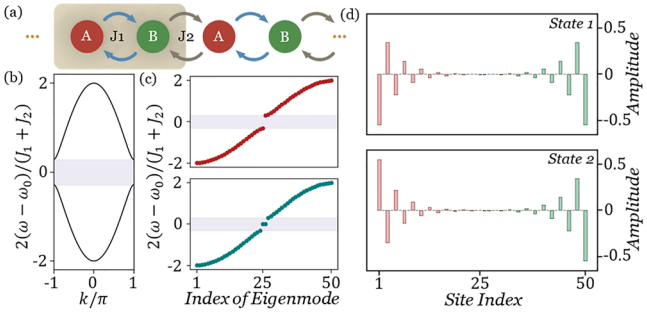

Figure 1. (a) Schematic of the SSH bath. The photonic lattice consists of two sublattices A (red) and B (green). The intracell hopping rate is J_1 and intercell hopping rate is J_2. (b) Dispersion relation of the SSH bath where the shaded region denotes the band gap. (c) Resonant frequencies of a finite bath consisting of $N = 50$ sites. Trivial phase (red) is characterized by $J_1 > J_2$, whereas the topological phase (blue) characterized by $J_1 < J_2$. (d) Wave function of the hybridized edge modes of a topological bath with $N = 50$ sites. Left edge state is localized on sublattice A (red); right edge state is localized on sublattice B (green).

where $a_i^\dagger(a_i)$ and $b_i^\dagger(b_i)$ denote the site bosonic creation (destruction) operators at site A and B of the i^{th} unit cell. Assuming periodic boundary conditions the Hamiltonian in momentum space can be written as

$$\tilde{\mathcal{H}}_B(k) = \begin{bmatrix} \omega_0 & J_1 + J_2 e^{-jk} \\ J_1 + J_2 e^{jk} & \omega_0 \end{bmatrix} \tag{2}$$

The properties of this disorder free bath can be summarized as follows:

(i) The bath has a chiral symmetry[25] owing to which the eigenstates of the Hamiltonian $\tilde{\mathcal{H}}_B(k)$ form two symmetric bands about ω_0 given by

$$\omega_\pm(k) = \omega_0 \pm \sqrt{J_1^2 + J_2^2 + 2J_1J_2\cos(k)} \tag{3}$$

where the $\pm$ denotes the upper/lower pass bands (Figure 1b) with a band gap of $2|J_1 - J_2|$.

(ii) This bath supports topologically nontrivial phases[25] depending on whether $J_1 < J_2$, which is termed as the topological phase, or $J_1 > J_2$, which is termed as the "trivial" phase. In a finite bath, these phases lead to formation of topological states localized at the edges of the lattice with an exponential decay into the bulk.[20,25] These edge states lie in the middle of the band gap centered around ω_0 for the topological phase and disappear for the trivial phase (Figure 1c). They have nonvanishing amplitude over only one of the two sublattices A or B and the small amount of overlap in the bulk causes these edge modes to hybridize as even and odd eigenstates of the system (Figure 1d).

(iii) Bello et al.[8] and Kim et al.[12] have shown that if a quantum emitter with transition frequency lying at the center of band gap (ω_0) is coupled to a site of this SSH bath, the resulting photonic bound state mimics an effective topological edge state in middle of the bath. This bound state inherits all the properties of the topological edge states, localizing the photon to one direction and sublattice depending on the site type (A or B) to which the emitter is coupled. In the presence of several emitters, these states can be used to mediate directional, topological interactions between them, which can give rise to exotic many body phases.

EFFECTS OF FABRICATION DISORDER

These properties, which are critical to realize unconventional quantum phenomena using the topological bath are adversely affected in the presence of fabrication disorder. In the optical domain, a scalable implementation of the SSH bath relies on nanofabrication to create solid state optical cavity arrays. The major form of disorder that exists in solid state photonic systems is in the resonance frequencies of the cavities arising from the inconsistencies in lithography and etching as well as from the nonuniformities in the film thickness of the bare wafer itself. This disorder is modeled by modifying the diagonal terms of the Hamiltonian to include random δ_is drawn from a zero-mean Gaussian distribution with a standard deviation σ.[26,27] Thus, the modified bath's Hamiltonian in the presence of this diagonal disorder can be written as

$$\mathcal{H}_B^\sigma = \mathcal{H}_B + \sum_i (\delta_{a,i} a_i^\dagger a_i + \delta_{b,i} b_i^\dagger b_i) \tag{4}$$

It is straightforward to see that the eigenproperties of this Hamiltonian depend on relative values of $J_1 - J_2$, σ, and $J_1 + J_2$. Hence, we define a dimensionless parameter

$$\eta = 2\sigma/(J_1 + J_2) \tag{5}$$

as the measure of relative disorder present in our system. We study the effect of the diagonal disorder on the key properties of the bath by looking at the evolution of topological bound states and the transmission spectrum as we sweep across σ, keeping J_1, J_2 constant (for a discussion on effects of off-diagonal disorder, see Section 1 of the Supporting Information).

As mentioned in property (iii), the presence of a quantum emitter lying in the middle of the band gap (ω_0) induces formation of bound directional states which are akin to topological edge states in their properties.[8] We first study the effect of disorder on this type of bound state.

In Figure 2, we consider a bath made of 50 resonators configured in trivial phase with a quantum emitter coupled to a type A site in the middle of the array. For this system, we plot the modulus of the amplitude of the induced bound state wave function averaged across 10^4 disorder realizations per η. Without any disorder, the bound state envelope extends toward the right direction and occupies only the B sublattice. Presence of diagonal disorder breaks the chiral symmetry of the Hamiltonian and protection to the bound state weakens. Despite this, in the region where $\eta \ll 1$, the bound exists with strong localization toward one direction and vanishing amplitudes on the conjugate sublattice. As the value η increases, the bound state becomes more delocalized and has weights over both the sublattices. When $\eta \to 1$ overall averaged bound state wave function over different realizations is spread across the array and loses all of its topological properties.

Fabricated photonic baths are experimentally characterized by measuring the transmission spectrum $|S_{21}|^2$ as relevant bath parameters can be extracted in a straightforward manner from such a measurement. To observe the effect of disorder on the transmission spectrum; we simulate and plot $|S_{21}|^2$ of a photonic bath with eight sites for both topological and trivial phases, again averaging across 10^4 disorder realizations per η

https://doi.org/10.1021/acsphotonics.1c01751
ACS Photonics XXXX, XXX, XXX−XXX

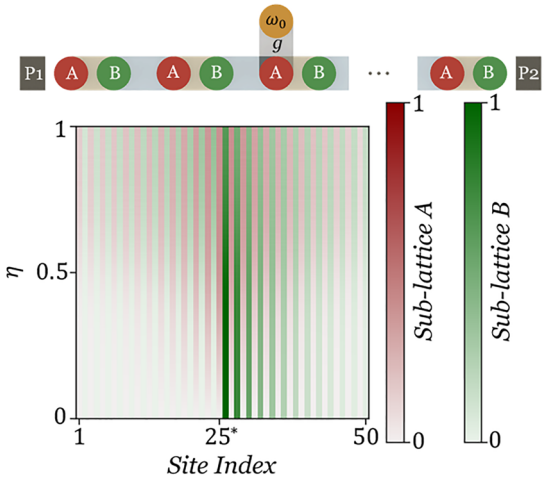

Figure 2. Modulus of amplitude of bound state wave function (normalized) as we sweep across η averaging over 10^4 disorder realizations per η. The schematic depicts a quantum emitter coupled to a SSH bath in trivial phase (J_1/J_2 = 1.336) at a site of sublattice A. The coherent emitter-cavity coupling rate is $g = (J_1 + J_2)/10$. In absence of any disorder, the bound state is localized toward the right with nonzero amplitude on sublattice B only. The direction of this envelope changes if the emitter is coupled to sublattice B instead of A. 25* denotes the position of the emitter in the array. Amplitudes on sublattice A are in red and on sublattice B are in green.

(Figure 3). The first thing that becomes immediately obvious is that the transmission amplitude of the farthest modes from

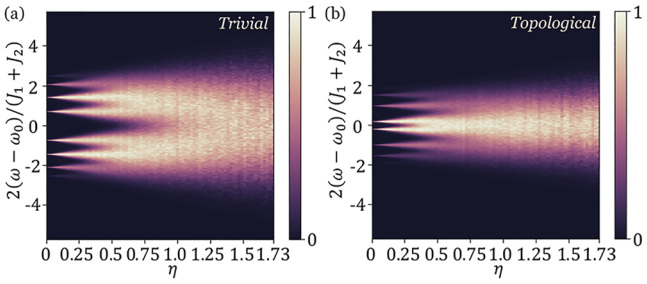

Figure 3. Transmission spectrum $|S_{21}|^2$ of a photonic bath with eight sites; averaged across 10^4 disorder realizations per η: (a) Trivial phase (J_1/J_2 = 1.336); (b) Topological phase (J_2/J_1 = 1.336).

the bare resonance is rather small, even when $\eta = 0$. This comes out naturally in the process of solving a set of coupled mode equations and combining it with the input−output formalism to express output field in terms of input fields (see Section 2 of Supporting Information). When the disorder is added to this model, we find that the transmission of the farthest modes gets rapidly less prominent even in the region $\eta \ll 1$. Consequently, probing all super modes becomes very difficult in a cavity array with large number of sites. As the value of η further increases the modal peaks start to merge, and in the region with $\eta \gg 1$, the averaged plot approaches a broad Gaussian distribution. This behavior clearly indicates that $\eta < 1$ is a necessary condition when using the transmission spectrum for accurately identifying eigenmodes of the simulated Hamiltonian and calculating relevant parameters like location and size of band gaps which play a critical role in determining quantum properties of the system (for further discussion, see Section 3 of Supporting Information). Thus, looking at the behavior of both the topological bound states and the transmission spectrum with increasing disorder, we can conclude that operating in the regime $\eta \ll 1$ can mitigate the effects of inherent fabrication disorder and allows us to harness the unconventional topological properties of the SSH bath. This can be achieved by designing the bath such that individual sites have much larger hopping rates than the disorder.

RESULTS

To realize these baths, we implemented the photonic analog of SSH model as coupled cavity arrays made from racetrack resonators fabricated in silicon photonics with 220 nm thick Si layer on a 3 μm thick SiO_2 film (Figure 4a). Each device is probed via a set of grating couplers located at the first and last site to coherently measure its transmission and reflection spectra. A similar platform has been used before[16] to show the existence of higher order edge states in photonic lattices. Those devices were operated in regime where localization lengths of the edge states were extremely small ($J_2/J_1 \gg 1$) and the band gap ($2|J_1 - J_2|$) size was similar to the disorder magnitude. But their disorder to hopping rates ratio was η = 1.95, which is $\gg$1. While edge states can be observed in this regime, as discussed above, it is not suitable for enabling bath-mediated directional interactions between emitters for quantum simulation purposes (see Section 3 of Supporting Information for further discussion). In order to reach the regime of $\eta \ll 1$, we need to increase the absolute value of hopping rates between the lattice sites. Hopping rates between optical cavities depend on the mode overlap of the two resonators $J \propto e_1^* e_2$,[28,29] where e_1 and e_2 denote mode volume normalized field profiles of the resonator modes. This overlap can be increased in broadly three ways: (1) by reducing the physical distance between sites, (2) by increasing the length of coupling region between the resonators, and (3) by reducing their mode volumes. Resolution of the lithography process limits the closest gap we can place two resonators without introducing additional disorder. Therefore, to increase the hopping rates further we need to reduce the size of resonators and increase the length of interaction region between them. To this end, we fabricated device arrays made up of racetrack resonators, which are 60 μm long with a 12 μm long coupling region. To obtain two differing hopping rates between the resonators, we kept the inter-resonator gap to be either 90 or 110 nm. The shorter length of the racetrack resonators not only helps in the reduction of the mode volume, but also ensures a large free spectral range for the devices to prevent interaction between different longitudinal modes of the same resonator.

Then, we measured the transmission spectrum of these devices. It is well-known that the devices fabricated on different parts of the chip are more susceptible to disorder and suffer from an overall mean frequency shift owing to variations in nanofabrication processes across the chip area.[18,26,27] We label this as the global disorder and characterized it via a statistical study of spectral modes across devices and tracking their mean frequency (Table 1). We fabricated arrays with varying number of racetrack resonator sites ranging from 1 to 16 on the same chip. Only devices in which we could spectrally resolve all the modes, were used to calculate the disorder. Usually this global disorder, calculated from statistics of the mean frequency of modes is subtracted from the spectrum as an overall shift to the origin.[26] This approach is strictly valid only if we are dealing with arrays that have small footprint on a

https://doi.org/10.1021/acsphotonics.1c01751
ACS Photonics XXXX, XXX, XXX−XXX

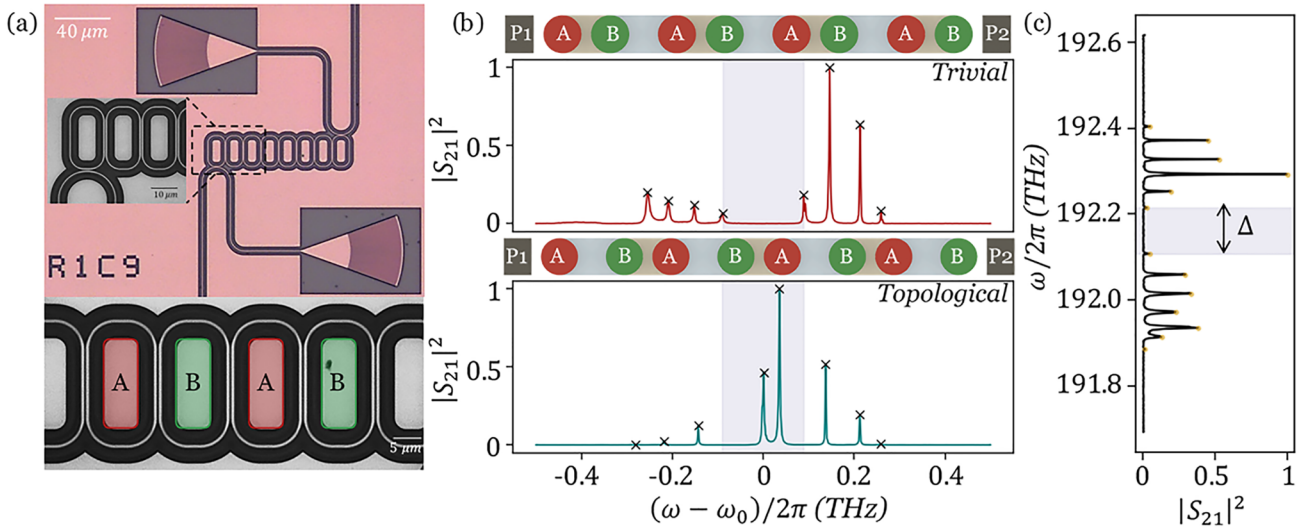

Figure 4. (a) Optical micrographs of a photonic SSH bath. (b) Normalized transmission spectrum of a SSH photonic bath with eight sites. Upper plot (red) depicts the trivial phase, whereas the lower plot (blue) depicts the topological phase. We can observe the band gap (shaded) formation in trivial phase, and the existence of edge modes in middle of the band gap in topological phase. The schematic depicts the ports, that is, the grating couplers used for transmission measurement. (c) A SSH photonic bath made of 8 unit cells, that is, 16 sites in trivial phase. Measured band gap is Δ = 0.107 THz, which closely matches the theoretical prediction of 0.11 THz.

Table 1. Disorder Compilation of the SSH Photonic Bath, $J_1/2\pi$ = 163 GHz, $J_2/2\pi$ = 122 GHz

σ_{type}	$\sigma/2\pi$ (GHz)	η	# measured
global	70.68	0.49	25
local	8.02	0.056	18

chip. As the cavity arrays have an increasing number of sites, the device area starts to grow, and therefore within one big device global disorder cannot just be ignored as an overall origin shift.

We also calculated and characterized local disorder which persists even after shifting the spectra to a common origin. To calculate this disorder, we measured the deviation of each individual mode across instances of similar devices across the chip:

$$\sigma_{\text{local}} = \frac{1}{2\pi}\sqrt{\sum \frac{(\omega_i - \omega_i^{\text{mean}} - \omega_{\text{shift}}^{\text{g}})^2}{n}} \tag{6}$$

where ω_i is the frequency of the i^{th} supermode, $\omega_{\text{shift}}^{\text{g}}$ is the global frequency shift to align the origins and ω_i^{mean} is the mean position of the supermode across the same device design made at different locations of the chip. This method allowed us to combine statistical data for disorder from devices with various number of sites and with varying phases (topological/trivial). The calculated value of η for local disorder was 0.056 ($\ll$1). Further details of the fabricated baths, their measured spectra and disorder distribution can be found in Section 4 of Supporting Information.

The larger hopping rates present in these arrays allow for reduction of the effects of disorder. In lattices with up to eight sites, we observe spectral accessibility to all the modes and global disorder has minimal effects on devices. This allows for clear comparison of band gap formation in the case of trivial phase and existence of two edge modes lying inside the band gap in the topological phase (Figure 4b). For photonic baths with more than eight sites all modes are not clearly observable due to vanishing amplitudes further away from the mean frequency and increasing effects of global disorder on the spectrum. Despite this, the device design allows for realization of photonic baths (here, trivial phase) with up to 16 sites (Figure 4c). We can observe a clear band gap formation with Δ = 0.107 THz, which is within 3% of the theoretical prediction. As discussed before such a photonic bath can be used to endow several special properties to coupled emitters also described in detail by Bello et al.[8]

CONCLUSION

In conclusion, using coupled cavity arrays we experimentally demonstrated topological photonic baths which are optical analogs of the SSH model. We studied the effect of fabrication induced disorder on these baths and demonstrated the steps required to overcome its effects. A similar, more detailed demonstration has been reported in superconducting systems[12] and our work enables a way to bring such topological baths to optics by developing a paradigm to harness recent advancements made in topological photonics and applying them to quantum simulation in optical domain. Future work will include independent tuning of each resonator site in the array to tackle global disorder effects and integration of quantum emitters[30] with the photonic baths to probe topological quantum phenomena.

ASSOCIATED CONTENT

Supporting Information

The Supporting Information is available free of charge at https://pubs.acs.org/doi/10.1021/acsphotonics.1c01751.

Effects of off-diagonal disorder on SSH photonic bath, derivation of transmission spectrum of photonic baths, discussion on additional properties of SSH baths, disorder plots depicting deviations in mode frequencies, and additional optical micrographs of baths in trivial and topological phase (PDF)

https://doi.org/10.1021/acsphotonics.1c01751
ACS Photonics XXXX, XXX, XXX−XXX

AUTHOR INFORMATION

Corresponding Authors

Abhi Saxena − *Department of Electrical and Computer Engineering, University of Washington, Seattle, Washington 98195, United States;* orcid.org/0000-0001-6453-929X; Email: abhi15@uw.edu

Arka Majumdar − *Department of Electrical and Computer Engineering and Department of Physics, University of Washington, Seattle, Washington 98195, United States;* orcid.org/0000-0003-0917-590X; Email: arka@uw.edu

Authors

Yueyang Chen − *Department of Electrical and Computer Engineering, University of Washington, Seattle, Washington 98195, United States;* orcid.org/0000-0002-4390-550X

Zhuoran Fang − *Department of Electrical and Computer Engineering, University of Washington, Seattle, Washington 98195, United States;* orcid.org/0000-0001-8724-6633

Complete contact information is available at: https://pubs.acs.org/10.1021/acsphotonics.1c01751

Funding

The research was supported by National Science Foundation Grant NSF-QII-TAQS-1936100 and National Science Foundation Grant NSF-1845009.

Notes

The authors declare no competing financial interest.

ACKNOWLEDGMENTS

Part of this work was conducted at the Washington Nanofabrication Facility/Molecular Analysis Facility, a National Nanotechnology Coordinated Infrastructure (NNCI) site at the University of Washington, which is supported in part by funds from the National Science Foundation (Awards NNCI-1542101, 1337840, and 0335765), the National Institutes of Health, the Molecular Engineering and Sciences Institute, the Clean Energy Institute, the Washington Research Foundation, the M. J. Murdock Charitable Trust, Altatech, ClassOne Technology, GCE Market, Google, and SPTS.

REFERENCES

(1) Georgescu, I. M.; Ashhab, S.; Nori, F. Quantum simulation. *Rev. Mod. Phys.* **2014**, *86*, 153.

(2) Bello, M.; Platero, G.; González-Tudela, A. Spin many-body phases in standard and topological waveguide QED simulators. *arXiv:2106.11637 [quant-ph]* **2021**, na.

(3) Douglas, J. S.; Habibian, H.; Hung, C.-L.; Gorshkov, A. V.; Kimble, H. J.; Chang, D. E. Quantum many-body models with cold atoms coupled to photonic crystals. *Nat. Photonics* **2015**, *9*, 326−331.

(4) Manzoni, M. T.; Mathey, L.; Chang, D. E. Designing exotic many-body states of atomic spin and motion in photonic crystals. *Nat. Commun.* **2017**, *8*, 1−9.

(5) González-Tudela, A.; Hung, C.-L.; Chang, D. E.; Cirac, J. I.; Kimble, H. Subwavelength vacuum lattices and atom−atom interactions in two-dimensional photonic crystals. *Nat. Photonics* **2015**, *9*, 320−325.

(6) Roushan, P.; Neill, C.; Tangpanitanon, J.; Bastidas, V. M.; Megrant, A.; Barends, R.; Chen, Y.; Chen, Z.; Chiaro, B.; Dunsworth, A.; et al. Spectroscopic signatures of localization with interacting photons in superconducting qubits. *Science* **2017**, *358*, 1175−1179.

(7) Kollár, A. J.; Fitzpatrick, M.; Houck, A. A. Hyperbolic lattices in circuit quantum electrodynamics. *Nature* **2019**, *571*, 45−50.

(8) Bello, M.; Platero, G.; Cirac, J. I.; González-Tudela, A. Unconventional quantum optics in topological waveguide QED. *Sci. Adv.* **2019**, *5*, No. eaaw0297.

(9) Anderson, B. M.; Ma, R.; Owens, C.; Schuster, D. I.; Simon, J. Engineering topological many-body materials in microwave cavity arrays. *Phys. Rev. X* **2016**, *6*, No. 041043.

(10) Viyuela, O.; Rivas, A.; Gasparinetti, S.; Wallraff, A.; Filipp, S.; Martín-Delgado, M. A. Observation of topological Uhlmann phases with superconducting qubits. *npj Quantum Inf.* **2018**, *4*, 1−6.

(11) Wang, X.; Liu, T.; Kockum, A. F.; Li, H.-R.; Nori, F. Tunable Chiral Bound States with Giant Atoms. *Phys. Rev. Lett.* **2021**, *126*, No. 043602.

(12) Kim, E.; Zhang, X.; Ferreira, V. S.; Banker, J.; Iverson, J. K.; Sipahigil, A.; Bello, M.; González-Tudela, A.; Mirhosseini, M.; Painter, O. Quantum electrodynamics in a topological waveguide. *Phys. Rev. X* **2021**, *11*, No. 011015.

(13) Arrazola, J.; Bergholm, V.; Brádler, K.; Bromley, T.; Collins, M.; Dhand, I.; Fumagalli, A.; Gerrits, T.; Goussev, A.; Helt, L.; et al. Quantum circuits with many photons on a programmable nanophotonic chip. *Nature* **2021**, *591*, 54−60.

(14) Zhong, H.-S.; Wang, H.; Deng, Y.-H.; Chen, M.-C.; Peng, L.-C.; Luo, Y.-H.; Qin, J.; Wu, D.; Ding, X.; Hu, Y.; et al. Quantum computational advantage using photons. *Science* **2020**, *370*, 1460−1463.

(15) Hartmann, M. J. Quantum simulation with interacting photons. *J. Opt.* **2016**, *18*, 104005.

(16) Mittal, S.; Orre, V. V.; Zhu, G.; Gorlach, M. A.; Poddubny, A.; Hafezi, M. Photonic quadrupole topological phases. *Nat. Photonics* **2019**, *13*, 692−696.

(17) Mittal, S.; Fan, J.; Faez, S.; Migdall, A.; Taylor, J. M.; Hafezi, M. Topologically robust transport of photons in a synthetic gauge field. *Phys. Rev. Lett.* **2014**, *113*, No. 087403.

(18) Mittal, S. Topological Edge States in Silicon Photonics. *Ph.D. thesis*, Department of Electrical and Computer Engineering, University of Maryland, 2014.

(19) Hafezi, M.; Mittal, S.; Fan, J.; Migdall, A.; Taylor, J. Imaging topological edge states in silicon photonics. *Nat. Photonics* **2013**, *7*, 1001−1005.

(20) Parto, M.; Wittek, S.; Hodaei, H.; Harari, G.; Bandres, M. A.; Ren, J.; Rechtsman, M. C.; Segev, M.; Christodoulides, D. N.; Khajavikhan, M. Edge-mode lasing in 1D topological active arrays. *Phys. Rev. Lett.* **2018**, *120*, 113901.

(21) St-Jean, P.; Goblot, V.; Galopin, E.; Lemaître, A.; Ozawa, T.; Le Gratiet, L.; Sagnes, I.; Bloch, J.; Amo, A. Lasing in topological edge states of a one-dimensional lattice. *Nat. Photonics* **2017**, *11*, 651−656.

(22) Zhao, H.; Miao, P.; Teimourpour, M. H.; Malzard, S.; El-Ganainy, R.; Schomerus, H.; Feng, L. Topological hybrid silicon microlasers. *Nat. Commun.* **2018**, *9*, 1−6.

(23) Afzal, S.; Zimmerling, T. J.; Ren, Y.; Perron, D.; Van, V. Realization of anomalous Floquet insulators in strongly coupled nanophotonic lattices. *Phys. Rev. Lett.* **2020**, *124*, 253601.

(24) Su, W. P.; Schrieffer, J. R.; Heeger, A. J. Solitons in Polyacetylene. *Phys. Rev. Lett.* **1979**, *42*, 1698−1701.

(25) Asbóth, J. K.; Oroszlány, L.; Pályi, A. A short course on topological insulators. *Lect. Notes Phys.* **2016**, *919*, 997−1000.

(26) Underwood, D. L.; Shanks, W. E.; Koch, J.; Houck, A. A. Low-disorder microwave cavity lattices for quantum simulation with photons. *Phys. Rev. A* **2012**, *86*, No. 023837.

(27) Majumdar, A.; Rundquist, A.; Bajcsy, M.; Dasika, V. D.; Bank, S. R.; Vučković, J. Design and analysis of photonic crystal coupled cavity arrays for quantum simulation. *Phys. Rev. B* **2012**, *86*, 195312.

(28) Haus, H. A.; Huang, W. Coupled-mode theory. *Proc. IEEE* **1991**, *79*, 1505−1518.

(29) Smith, K. C.; Chen, Y.; Majumdar, A.; Masiello, D. J. Active tuning of hybridized modes in a heterogeneous photonic molecule. *Phys. Rev. Appl.* **2020**, *13*, No. 044041.

(30) Chen, Y.; Ryou, A.; Friedfeld, M. R.; Fryett, T.; Whitehead, J.; Cossairt, B. M.; Majumdar, A. Deterministic positioning of colloidal

quantum dots on silicon nitride nanobeam cavities. *Nano Lett.* **2018**, *18*, 6404−6410.

https://doi.org/10.1021/acsphotonics.1c01751
ACS Photonics XXXX, XXX, XXX−XXX